Shahrood University of Technology

Journal of Mining and Environment (JME)

Journal homepage: www.jme.shahroodut.ac.ir

Iranian Society of Mining Engineering (IRSME)

Numerical Study of Behavior of Eccentric-inclined Loaded Strip Footing Resting above a Soil Mass Containing a Void

Vaibhav Sharma*, Andy Kwame Yeboah, Joshua Asare, Natillio Pillay, Jaspreet Singh

Lovely Professional University, Phagwara, Punjab, India

Article Info

Received 16 May 2023

Received in Revised form 2 June 2023

Accepted 6 June 2023

Published online 6 June 2023

DOI:10.22044/jme.2023.13136.2390

Keywords

Underground Voids

Strip Footing

Eccentric-inclined Loading

Numerical Modeling

Geo-synthetics

Abstract

The presence of any underground cavity in the soil stratum can seriously harm the structural performance of the overlying facility. These may develop because of mining, tunneling, water, and gas networks or outdated channels. In the present investigation, a circular void is considered, and its effect on the surface strip footing (in the form of ultimate load (UL), ultimate settlement (US), footing tilting, and footing horizontal displacement (HD)) is studied using numerical simulation. The variable parameters are load eccentricity (e), load inclination (α), and geogrid reinforcement location (u). It is observed that as the load inclination and eccentricity increases, the UL decreases. For instance, in the unreinforced soil, u/B = 0, at load inclination of α = 0°, 10°, 20°, and 30°, the UL is 249, 200, 142, and 97 kN/m, respectively. Moreover, as the geo-grid location is changed, the UL first increases when placed near the footing (u/B = 0.10), and thereafter, starts to decrease as the distance between footing and geo-grid increases. For instance, the UL is 249, 278, 267, 260, 259, and 256 kN/m when e/B = 0.0, α = 0°, and u/B varies from 0 to 0.5 with an increment of 0.1. The tilting increases as the eccentricity is increased; for example, u/B = 0.0 for α = 0°; the tilting values are 0°, 0.12°, 0.31°, and 0.61°. Moreover, as the load eccentricity increases, the HD decreases (for u/B = 0.1 and α = 10°, the HD is 4.20, 3.5, 3.00, and 2.60 mm, respectively.

1. Introduction

Underground cavities or voids can get formed naturally as well as anthropogenically. Natural causes are mainly due to the presence of soluble rocks, in particular, carbonate rocks such as limestone, gypsum and dolomite. On the other hand, mineral extraction (due to mining activity) and tunnel construction (for roadway, railway, utilities such as liquid or gas transport and electrical supplies, etc.) are the anthropogenic causes of the formation of underground voids [1, 2]. Their presence can significantly affect the load-carrying capacity of the soil situated over it, which consequently, directly affect the stability of any overlying infrastructure.

With the increase in population, the land use and urbanization of most of the unexplored areas is increasing. The newly developed land may contain abandoned underground cavities or caves that are unknown or forgotten due to carelessness or lack of updated information. There are many studies available in the literature that clearly reported the collapse of underground caves, and thereby significantly affecting the urbanized area [3–11]. Fiore *et al.* [3], through a case study, presented the potential hazards posed by the occurrence of sinkholes in the southern region of Italy, Apulian. It was reported that the sinkholes were the result of developed instabilities in the existing underground voids. Yang *et al.* [4] presented the data of the past twelve years focusing on the investigations conducted on the presence of large Longyou rock caverns that were carved in argillaceous siltstone around 2000 years ago located in Longyou County in the middle of Quzhou — Jinhua Basin, Zhejiang Province, East China. The main objective of the study was to act as a reminder that a few of the relic sites experienced severe deterioration and could result in the collapse of entire rooftop. Vattano *et*

✉ *Corresponding author: civil.vaibhav.sharma@gmail.com (V. Sharma)*

al. [5] conducted field surveys, structural analysis, and numerical modeling of the fissured networks in the rock-mass in Sicily and Apulia regions of Southern Italy, to understand the factors responsible for the instability processes of underground quarries. It was reported that the occurrence of sinkholes is due to the saturation of calcarenite and the presence of various discontinuities in the rock-mass. Van Den Eeckhaut *et al.* [6] reported the formation of sinkhole due to the presence of underground limestone quarry with the help of a case study (South Limburg, Belgium). Parise and Lollino [7] investigated the effect of local instabilities occurring in the underground caves and their consequent failure mechanisms through numerical analysis. Furthermore, the results obtained from numerical simulation were compared with the field explorations. Castellanza *et al.* [10] proposed a methodological procedure for assessing the hazards associated with the underground abandoned caves. The proposed approach was further validated by comparing it with the real case studies. Song *et al.* [11] presented a case study, focusing on the identification, remediation and the analysis on the occurrence of sinkholes, under the longest railroad tunnel located in north-east region of South Korea.

There are a number of available solutions, but are not limited to, which can mitigate the issue of subsidence of the infrastructure lying over the soil mass containing voids are filling the voids with appropriate materials (grouting) [12, 13], using piles or caissons to bridge the voids [14], excavating and establishing a basis at the lowest level of the void [15], relocating the foundation and the use of geosynthetics. There are a few studies focusing on the stability improvement of the infrastructure situated over a soil mass containing voids using geo-synthetics [1, 2, 16, 17]. Cooper and Saunders [2] presented a solution to construct road and bridge across gypsum Krast in England. The roadway embankment was reinforced using tensile membrane that will prevent its sudden collapse, but will indicate the location of where problem exists. To prevent the failure of bridge, the foundations and the piers adjacent to the critical pier were enlarged and made more stronger with a view that, if any failure occurs in the critical region, the adjacent strong piers will carry its load, and hence, prevent a catastrophic failure. Jao and Wang [17] numerically studied the behavior of strip footing resting on soft ground containing concrete-lined tunnel. The variable parameters in the study were, tunnel location, tunnel size and lining thickness. It was suggested that the presence of lined-tunnel in soft ground can significantly increase the load-carrying capacity of surface strip footing. Tahmasebipoor *et al.* [1] suggested that the provision of geo-textile under the footing can significantly improve the load-carrying capacity of footing resting on soil mass containing voids. The factors influencing the load-carrying capacity were the geotextile's stiffness, location, number, and the spacing between adjacent layers of geotextiles. Very recently, Mazouz *et al.* [16] used numerical simulation to assess the effect of underground void on the strip footing resting on geogrid-reinforced sand slopes. It was reported that the presence of geogrid in the slope greatly improved its stability and the response of strip footing.

After conducting an extensive literature review, it was observed that most of the studies conducted in the past were only focused on the behavior of surface strip footing subjected to vertical-concentric load application. Hence, the present paper is focused on studying the behavior of surface strip footing subjected to different loading types (vertical-concentric, vertical-eccentric, inclined-concentric, and inclined-eccentric) resting on a soil mass containing a void. Three distinct parameters, load inclination (α), load eccentricity (e/B), and reinforcement location (u/B) were the focus of the study. The listed parameters together with other variables were simulated using the Finite Element Module (FEM), PLAXIS 2D. The simulations comprise two major components, unreinforced and geogrid-reinforced layouts. Therefore, the objectives of the present study are to understand the effect of inclined ($\alpha = 0^{\circ}$, 10°, 20°, and 30°) and eccentric (e/B = 0, 0.05, 0.10, and 0.15) load on a surface strip footing resting on soil mass containing void. Moreover, to understand the effect of geogrid location (u/B = 0, 0.1, 0.2, 0.3, 0.4, and 0.5) on the surface strip footing resting on soil mass containing void, a single geogrid layer was provided between the footing base and the crown of the void.

2. Numerical Software, Materials Used, and Numerical Modeling

In the present study, commercial FEM package, PLAXIS-2D is used. It is the most used 2D simulation tool in geo-technical engineering for the deformation and stability study of various construction stages that consider steady-state groundwater flow for saturated and partially saturated circumstances. Engineers use PLAXIS 2D as their go-to finite element analysis (FEA) application for everything from excavations, embankments, foundations, tunneling, mining, and reservoir geomechanics. It can quickly and effectively create models using present structural parts and loading types in a computer aided drafting (CAD)-like environment, giving more time to analyze the findings.

In the present study, elastic-perfectly plastic Mohr-Coulomb model was used for the soil. The soil used in the present study is a soft clay. The soil properties were entered in the *soils and interfaces* option available under the *material sets* in the *soil* tab of the PLAXIS-2D software. The properties of the soil used in the study are shown in Table 1 [17]. The geo-grid used in the study was modeled using an in-built option, *geo-grids* under *material sets*. Its properties used in the simulation are shown in Table 2 [18]. The footing was assumed to be made of concrete. It was modeled as a plate element and its properties used in the simulation are shown in Table 3.

Table 1. Soil properties.

Property	Values
Initial Modulus (kN/m^2)	19,843
Poisson's ratio	0.23
Dry unit weight (kN/m^2)	14.1
γ_{sat} (kN/m^3)	18.54
γ_{unsat} (kN/m^3)	14.10
Void ratio	0.5
Cohesion (kN/m^2)	158.5
Internal friction angle (˚)	8
Material model	Mohr-Coulomb

Table 2. Geo-grid properties.

Ultimate tensile strength (kN/m)	925
Width (m)	0.0025
Material type	Elastic

Table 3. Footing properties.

Footing width (m)	1.00
Footing thickness (m)	0.150
EI (kNm^2/m)	7702
EA_1 (kN/m)	4.11 x 10^6
Density of concrete (kN/m^3)	24.00

Figure 1 shows the schematic view of the simulation problem. A plane-strain analysis is considered in this study. A strip footing of 1m width is located at the surface of soil whose extent in vertical and horizontal direction is 5*B* and 10*B*, respectively, where *B* is the width of the strip footing. A circular void having diameter, *B* is considered in the soil mass. It was simulated using an inbuilt option, *create tunnels* under *structures* tab in PLAXIS-2D. In addition, a thickness of 150 mm was provided to the tunnel lining for the stability of the overlying soil. It is located at a distance of 2*B* (distance between the footing base and crown of the circular void) from the base of footing. Furthermore, to simulate the interaction of tunnel with the surrounding soil, geogrid with the surrounding soil and footing with the underlying soil, interface elements were generated. For footing and tunnels, only one interface element was generated; however, for geo-grid, two interface elements were generated. A point load, in the form of concentric-vertical, eccentric-vertical, concentric-inclined, and eccentric-inclined is applied on the strip footing. Out of the different meshing options available in PLAXIS-2D, a very fine mesh density was used in each simulation. The load eccentricity and inclination are represented by the symbol *e/B* and α, respectively. A geogrid of width, B_G, 2.5*B* is located at a varying depth (u = 0.1*B*, 0.2*B*, 0.3*B*, 0.4*B*, and 0.5*B*) below the footing. The footing, geogrid, and the voids are located in such a way that their geometric centers coincides with the center-line of the soil extent. The test plan considering the various variable parameters is shown in Table 4.

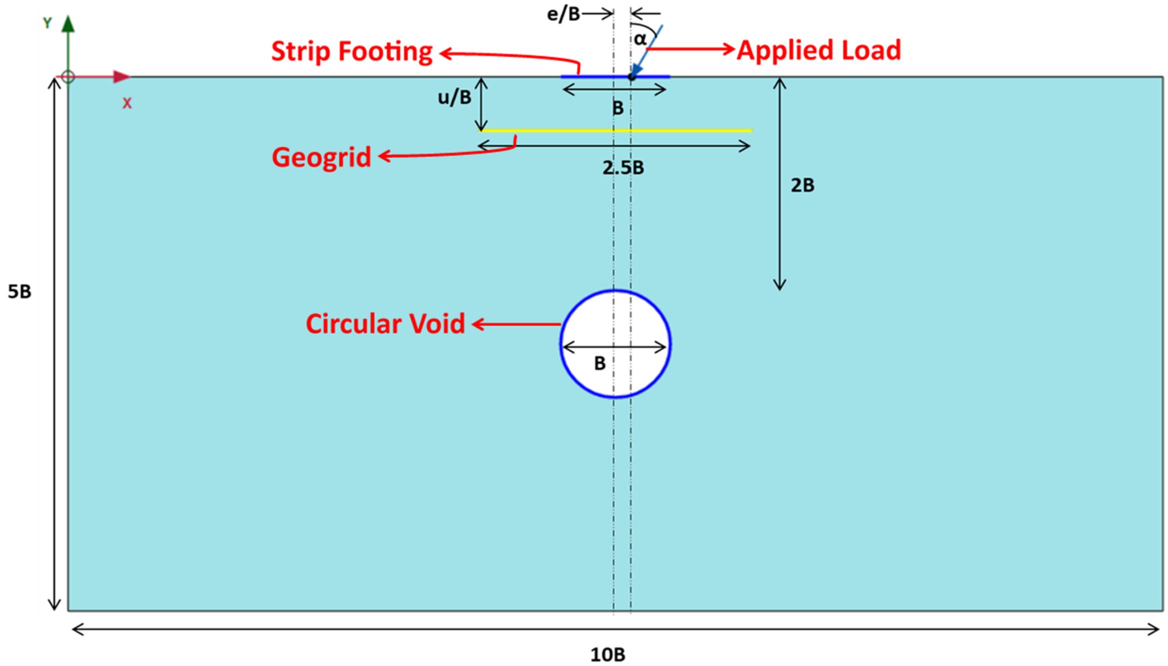

Figure 1. Schematic diagram of problem.

Table 4. Test plan.

Series	test type	Geo-grid location (u/B)	Load inclination (α)	Load eccentricity (e/B)
A	Unreinforced	--	0°, 10°, 20°, and 30°	0, 0.05, 0.10, and 0.15
B	Geo-grid reinforced	0.1, 0.2, 0.3, 0.4, and 0.5	0°, 10°, 20°, and 30°	0, 0.05, 0.10, and 0.15

3. Results and Discussion

This section of the paper shows and discusses the results obtained from the various simulations. The effect of load inclination, load eccentricity, and geo-grid location on the Ultimate Load (UL), Ultimate Settlement (US), footing tilting, and Footing Horizontal Displacement (HD) is presented and discussed. To determine the UL, the tangent intersection method has been used [19, 20] and the US is the settlement corresponding to the UL on the load-settlement curve. Footing tilting was obtained as the *tangent inverse* of the ratio of difference of US at the opposite edge of the footing to the width of the footing [21]. To determine the HD, the plot between Load-HD was used. It was obtained corresponding to the UL obtained using tangent intersection method, explained earlier.

3.1. Effect of load inclination

3.1.1. Effect of load inclination on UL

Figure 2 a-d shows the impact of load inclination on the UL. It is observed in Figure 2 that as the load inclination is increased the UL keeps on decreasing. For instance, Figure 2a, in the unreinforced soil; u/B = 0; at load inclination of α = 0°, 10°, 20°, and 30°, the UL is 249, 200, 142, and 97 kN/m, respectively. Similarly, in the case of reinforced soil (u/B = 0.1), the UL is 278, 235, 142, and 97 kN/m, respectively. A similar trend can be seen when u/B is 0.20, 0.30, 0.40, and 0.50. In Figure 2b, in the case of unreinforced soil, e/B= 0.05, at an inclination of α = 0°, α = 10°, α = 20°, α = 30° the UL is, 221, 191, 140, and 97 kN/m, respectively. Similarly, in the case of reinforced soil (u/B = 0.1), the UL is 246.5, 215, 140, and 96 kN/m, respectively. A similar trend can be seen when u/B is 0.20, 0.30, 0.40, and 0.50. In Figure 2c, in the case of unreinforced soil, e/B = 0.10, at inclination of α = 0°, α = 10°, α = 20°, α = 30°, the UL is 205, 175, 131, and 94 kN/m, respectively. Similarly, in the occurrence reinforced soil (u/B = 0.1); the UL is 230, 215, 133, and 95 kN/m, respectively. A related pattern can be seen when u/B is 0.20, 0.30, 0.40, and 0.50. In Figure 2d, in the occurrence of unreinforced soil, e/B = 0.15, at an inclination of α = 0°, α = 10°, α = 20°, α = 30°, the UL is 177, 159, 119, and 90 kN/m, respectively. Similarly, in the case of reinforced soil (u/B = 0.1), the UL is 196, 195, 122, and 91 kN/m, respectively. A comparable pattern is evident when u/B is 0.20, 0.30, 0.40, and 0.50.

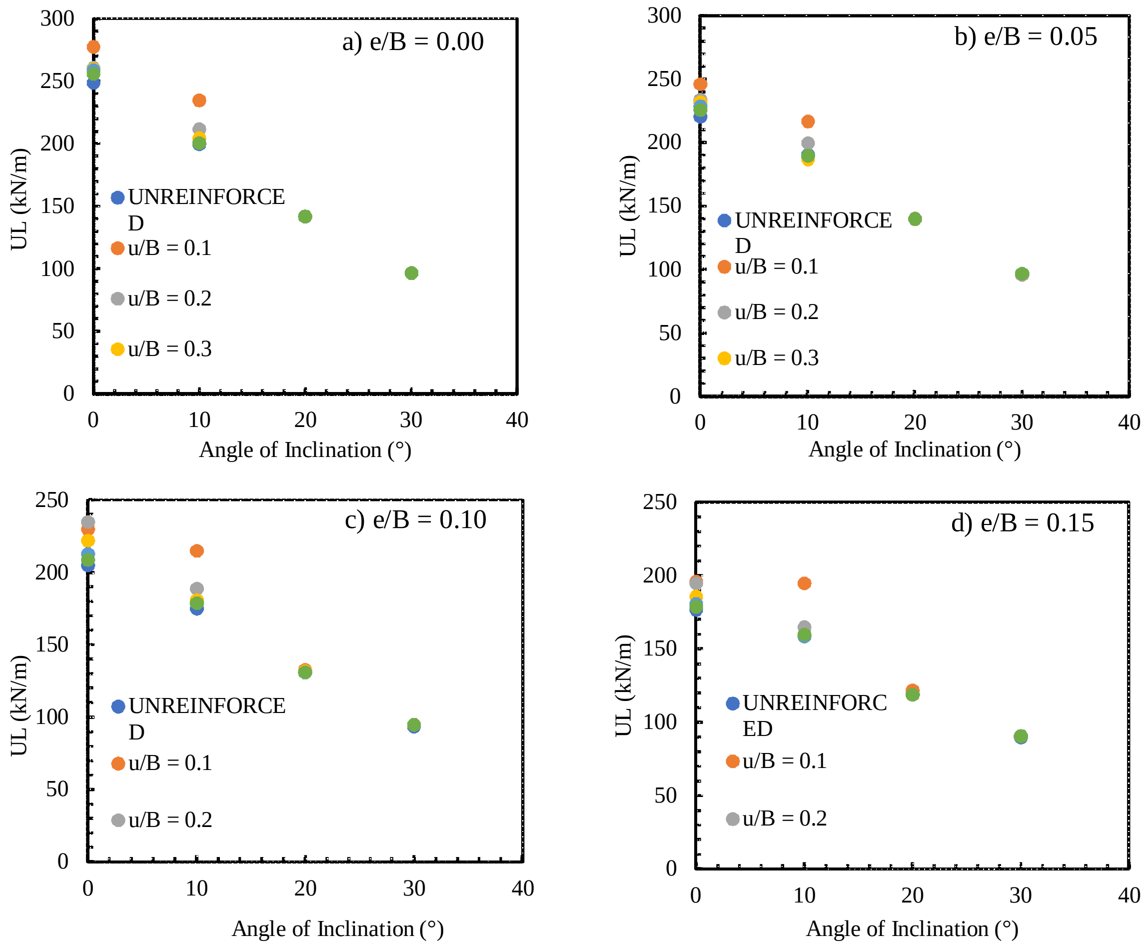

Figure 2. Influence of load inclination on the UL for various load eccentricity; a) e/B = 0.00, b) e/B = 0.05, c) e/B = 0.10, and d) e/B = 0.15.

3.1.2. Effect of load inclination on US

Figure 3 a-d shows the impact of load inclination on the US. It is apparent in Figure 3 that as the load inclination is increased the US keeps on decreasing. For instance, Figure 3a, in the case of unreinforced soil, e/B = 0.0, at an inclination of $\alpha = 0^{\circ}$, $\alpha = 10^{\circ}$, $\alpha = 20^{\circ}$, $\alpha = 30^{\circ}$, the US is 9.4, 8.75, 8.1, and 5.1 mm, respectively. Similarly, the case of reinforced soil (u/B = 0.1); the US is 11.25, 9.5, 8, and 5.52 mm, respectively. A comparable trend can be seen when u/B is 0.20, 0.30, 0.40, and 0.50. In Figure 3b, in the case of unreinforced soil, e/B= 0.05, at an inclination of $\alpha = 0^{\circ}$, $\alpha = 10^{\circ}$, $\alpha = 20^{\circ}$, $\alpha = 30^{\circ}$, the US is 8.95, 7.5, 8.08, and 5.12 mm, respectively. Similarly, in the case of reinforced soil (u/B = 0.1), the US is 10.25, 9.5, 7.81, and 5.18 mm, respectively. A comparable pattern is evident can be seen when u/B is 0.20, 0.30, 0.40, and 0.50. In Figure 3c, in the case of unreinforced soil, e/B= 0.10, at an inclination of $\alpha = 0^{\circ}$, $\alpha = 10^{\circ}$, $\alpha = 20^{\circ}$, $\alpha = 30^{\circ}$, the US is 8.3, 7.2, 7.6, and 5.1, respectively. Similarly, in the case of reinforced soil (u/B = 0.1), the US is 8.6, 9.25, 6.95, and 5.05, respectively. A similar trend can be seen when u/B is 0.20, 0.30, 0.40, and 0.50. In Figure 3d, in the case of unreinforced soil, e/B = 0.15, at an inclination of $\alpha = 0^{\circ}$, $\alpha = 10^{\circ}$, $\alpha = 20^{\circ}$, $\alpha = 30^{\circ}$, the US is 7.7, 6.95, 7.75, and 5.3 mm, respectively. Similarly, in the case of reinforced soil (u/B = 0.1), the US is 6.9, 8.9, 6.87, and 5.05 mm, respectively. Moreover, a similar trend can be seen when u/B is 0.20, 0.30, 0.40, and 0.50.

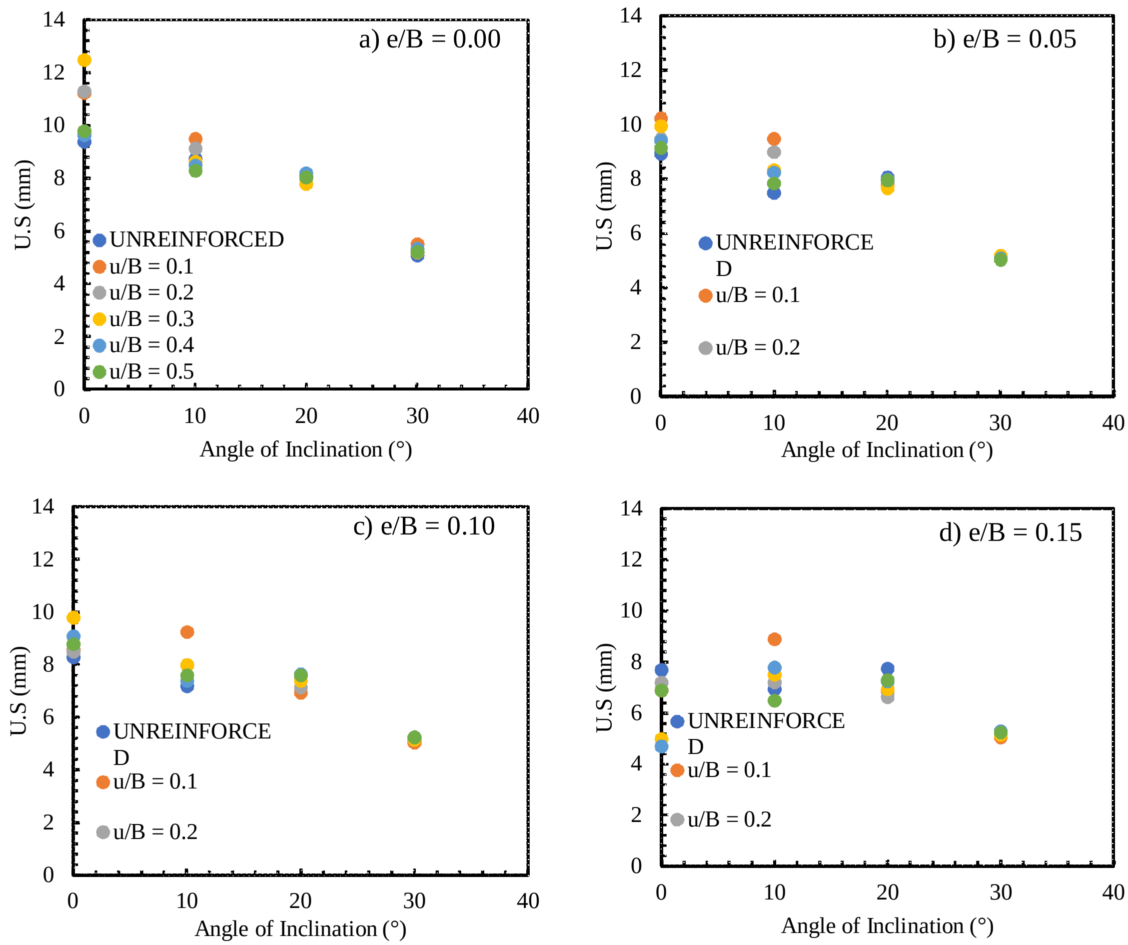

Figure 3. Impact of load inclination on the US for different load inclinations; a) e/B = 0.00, b) e/B = 0.05, c) e/B = 0.10, and d) e/B = 0.15.

3.1.3. Effect of load inclination on footing tilt

Figure 4 a-d shows the influence of load inclination footing tilting. It can be observed in Figure 4 that when the load inclination is increased the Footing tilting keeps on increasing from $\alpha = 0^{\circ}$ to $\alpha = 20^{\circ}$ and it sharply decreases at $\alpha = 30^{\circ}$. For instance, Figure 4a, in the case of unreinforced soil, u/B= 0, at load inclination of $\alpha = 0^{\circ}$, $\alpha = 10^{\circ}$, $\alpha = 20^{\circ}$, $\alpha = 30^{\circ}$, the tilting angle is 0°, 0.07°, 0.1°, and 0.03°, respectively. Similarly, for the case of reinforced soil (u/B = 0.1), the tilting angle is 0°, 0.06°, 0.11°, and -0.00144°, respectively. A similar trend can be seen when u/B is 0.20, 0.30, 0.40, and 0.50. In Figure 4b, in the case of unreinforced soil, e/B = 0.05, at an inclination of $\alpha = 0^{\circ}$, $\alpha = 10^{\circ}$, $\alpha = 20^{\circ}$, $\alpha = 30^{\circ}$, the tilting angle is 0.12°, 0.09°, 0.08°, and 0.03°, respectively. Similarly, in the case of reinforced soil (u/B = 0.1), the tilting angle is 0.09°, 0.08°, 0.06°, and 0.04°, respectively. A related pattern can be seen when u/B is 0.20, 0.30, 0.40, and 0.50. In Figure 4c, in the case of unreinforced soil, e/B= 0.10, at an inclination of $\alpha = 0^{\circ}$, $\alpha = 10^{\circ}$, $\alpha = 20^{\circ}$, $\alpha = 30^{\circ}$, the tilting angle is 0.31°, 0.21°, 0.23°, and 0.09°, respectively. Similarly, in the case of reinforced soil (u/B = 0.1); the tilting angle is 0.2°, 0.14°, 0.19°, and 0.09°, respectively. A parallel trend can be seen when u/B is 0.20, 0.30, 0.40, and 0.50. In Figure 4d, in the case of unreinforced soil, e/B = 0.15, at an inclination of $\alpha = 0^{\circ}$, $\alpha = 10^{\circ}$, $\alpha = 20^{\circ}$, $\alpha = 30^{\circ}$, the tilting angle is 0.61°, 0.29°, 0.32°, and 0.16°, respectively. Similarly, in the case of reinforced soil (u/B = 0.1), the Tilting angle is 0.58°, 0.25°, 0.27°, and 0.17°, respectively. A comparable pattern is evident when u/B is 0.20, 0.30, 0.40, and 0.50.

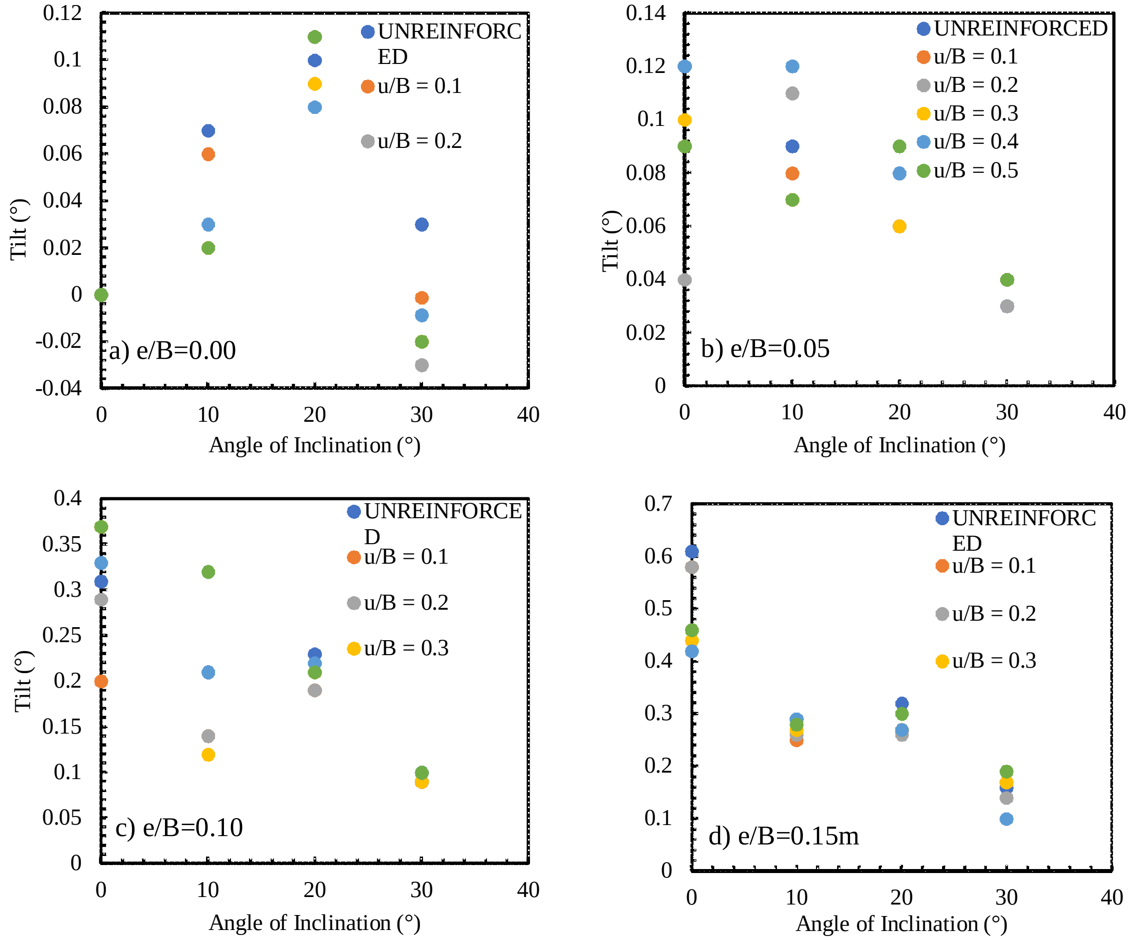

Figure 4. Impact of load inclination on the footing tilting for various load eccentricities; a) e/B = 0.00, b) e/B = 0.05, c) e/B = 0.10, and d) e/B = 0.15.

3.1.4. Effect of load inclination on HD

Figure 5 a-d shows the influence of load inclination on the HD. It can be seen in Figure 5 that it is obvious that as the load inclination is increased the HD keeps on increasing to $\alpha = 0^{\circ}$, and then decreases at $\alpha = 30^{\circ}$. For instance, Figure 5a, the case of unreinforced soil, u/B = 0, at load inclination of $\alpha = 0^{\circ}$, $\alpha = 10^{\circ}$, $\alpha = 20^{\circ}$, $\alpha = 30^{\circ}$, the HD is 0, 3.1, 6.13, and 4.79 mm, respectively. Similarly, with the case of reinforced soil (u/B = 0.1), the HD is 0, 3.15, 5.79, and 4.77 mm, respectively. A similar trend can be seen when u/B is 0.20, 0.30, 0.40, and 0.50. In Figure 5b, in the case of unreinforced soil, e/B= 0.05, at an inclination of $\alpha = 0^{\circ}$, $\alpha = 10^{\circ}$, $\alpha = 20^{\circ}$, $\alpha = 30^{\circ}$, the HD is 0, 3, 4.73, 4.95 mm, respectively. However, there was an increase throughout this pattern. Similarly, for the case of reinforced soil (u/B = 0.1), the HD is 0, 3.5, 5.99, and 5.01 mm, respectively. A similar trend can be seen when u/B is 0.20, 0.30, 0.40, and 0.50. In Figure 5c, in the case of unreinforced soil, e/B = 0.10, at an inclination of $\alpha = 0^{\circ}$, $\alpha = 10^{\circ}$, $\alpha = 20^{\circ}$, $\alpha = 30^{\circ}$, the HD is 0, 2.8, 5.62, and 5.05 mm, respectively. Similarly, in the case of reinforced soil (u/B = 0.1), the HD is 0, 3, 5.18, and 4.85 mm, respectively. A similar trend can be seen when u/B is 0.20, 0.30, 0.40, and 0.50. In Figure 5d, in the case of unreinforced soil, e/B= 0.15, at an inclination of $\alpha = 0^{\circ}$, $\alpha = 10^{\circ}$, $\alpha = 20°$, $\alpha = 30^{\circ}$, the HD is 0, 2.4, 5.49, and 4.97 mm, respectively. Similarly, in the case of reinforced soil (u/B = 0.1), the HD is 0, 2.6, 4.76, and 5.05 mm, respectively. A continuous increase was also observed at e/B = 0.15. A similar trend can be seen when u/B is 0.20, 0.30, 0.40, and 0.50.

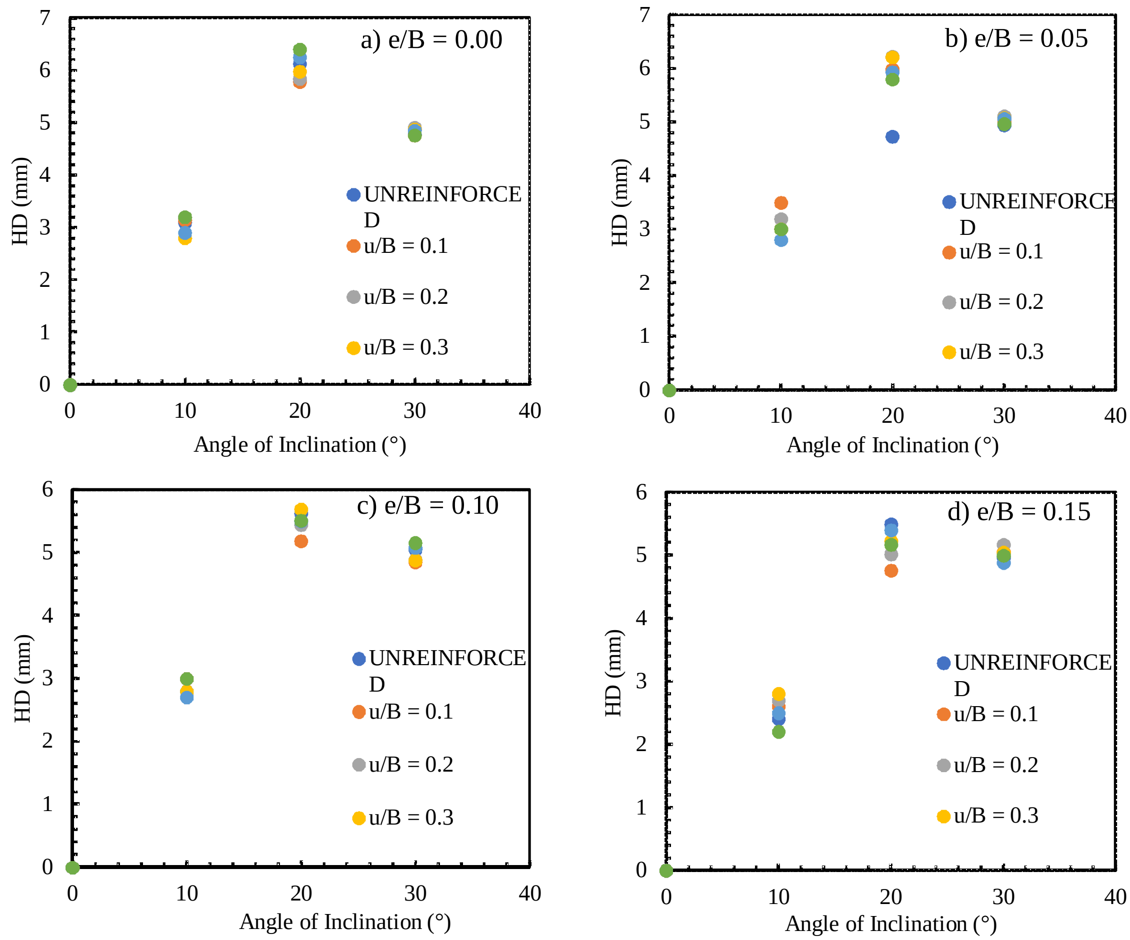

Figure 5. Relation of load inclination on the Footing horizontal displacement for various load eccentricities; a) e/B = 0.00, b) e/B = 0.05, c) e/B = 0.10, and d) e/B = 0.15.

3.2. Effect of Load eccentricity

3.2.1. Effect of load eccentricity on UL

Figure 6 a-d shows the impact of load eccentricity on the UL. It is obvious in Figure 6 that as the load eccentricity is increased the UL keeps on decreasing. For instance, Figure 6a, in the case of unreinforced soil, α = 0°, at load eccentricity of 0B, 0.05B, 0.10B, and 0.15B, the UL is 249, 221, 205, and 177 kN/m, respectively. Similarly, in the case of reinforced soil (u/B = 0.1), the UL is 278, 246.5, 230, and 196 kN/m, respectively. A corresponding trend can be seen when u/B is 0.20, 0.30, 0.40, and 0.50. In Figure 6b, in the case of unreinforced soil, α = 10°, at load eccentricity of 0B, 0.05B, 0.10B, and 0.15B, the UL is 200, 191, 175, and 159 kN/m, respectively. Similarly, in the case of reinforced soil (u/B = 0.1), the UL is 235, 217, 215, and 195 kN/m, respectively. A relatable pattern can be seen when u/B is 0.20, 0.30, 0.40, and 0.50. In Figure 6c, in the case of unreinforced soil, α = 20°, at load eccentricity of 0B, 0.05B, 0.10B, and 0.15B, the UL is 142, 140, 131, and 119 kN/m, respectively. Similarly, in the case of reinforced soil (u/B = 0.1), the UL is 142, 140, 133, and 122 kN/m, respectively. A corresponding trend can be seen when u/B is 0.20, 0.30, 0.40, and 0.50. In Figure 6d, in the incident of unreinforced soil, α = 30°, at load eccentricity of 0B, 0.05B, 0.10B, and 0.15B, the UL is 97, 97, 94, and 90 kN/m, respectively. Similarly, in the case of reinforced soil (u/B = 0.1); the UL is 97, 96, 95, and 91 kN/m, respectively. A clear-cut trend can be seen when u/B is 0.20, 0.30, 0.40, and 0.50.

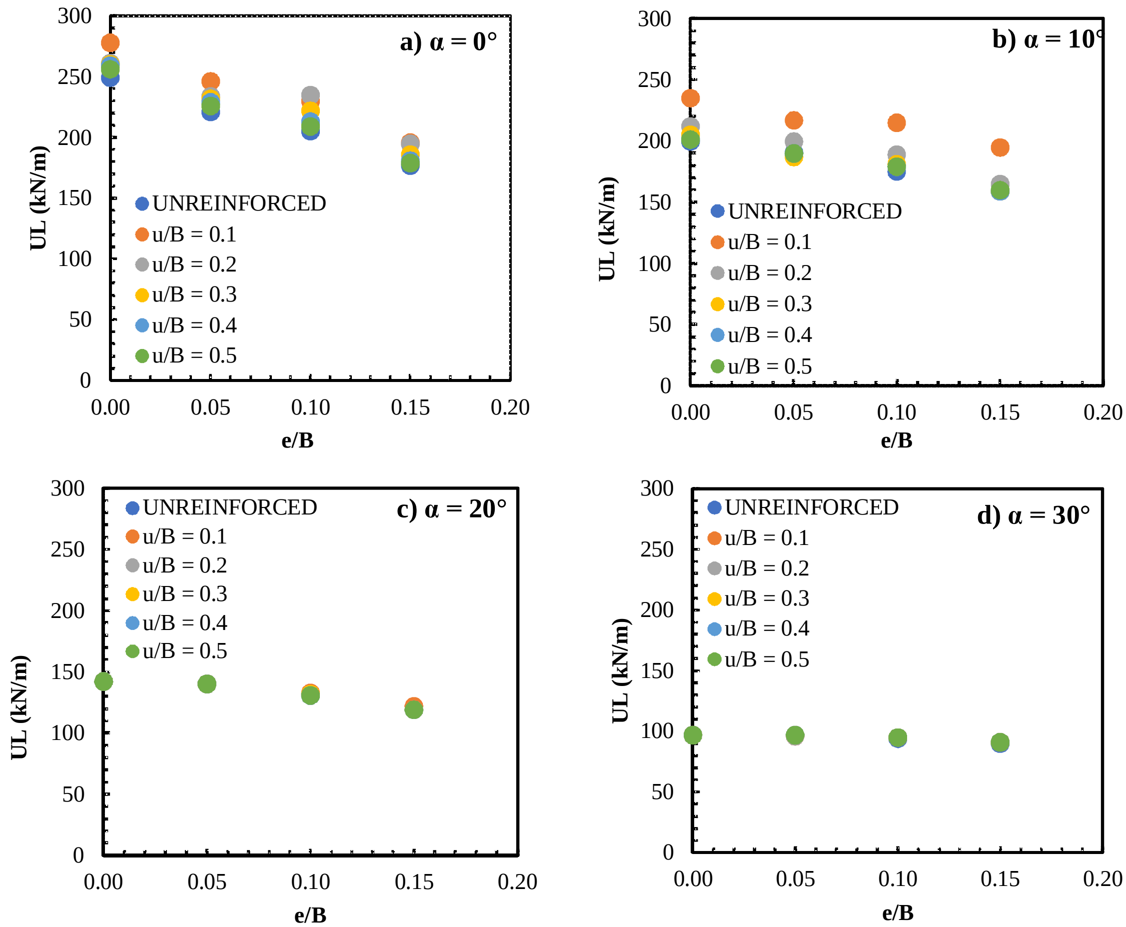

Figure 6. Effect of load eccentricity on the ultimate load for various load inclinations; a) α = 0˚, b) α = 10˚, c) α = 20˚, and d) α = 30˚.

3.2.2. Effect of load eccentricity on US

Figure 7 a-d shows the effect of load eccentricity on the US. It can be seen in Figure 7 that as the load eccentricity is increased the US keeps on decreasing. For instance, Figure 7a, in the case of unreinforced soil, α = 0˚, at load eccentricity of 0B, 0.05B, 0.10B, and 0.15B, the US is 9.40, 8.95, 8.30, and 7.70 mm, respectively. Similarly, in the case of reinforced soil (u/B = 0.1), the US is 11.25, 10.25, 8.60, and 6.90 mm, respectively. A similar trend can be seen when u/B is 0.20, 0.30, 0.40, and 0.50. In Figure 7b, in the case of unreinforced soil, α = 10˚, at load eccentricity of 0B, 0.05B, 0.10B, and 0.15B, the US is 8.75, 7.50, 7.20, and 6.95 mm, respectively. Similarly, in the case of reinforced soil (u/B = 0.1), the US is 9.50, 9.50, 9.25, and 8.90 mm, respectively. A similar trend can be seen when u/B is 0.20, 0.30, 0.40, and 0.50. In Figure 7c, in the case of unreinforced soil, α = 20˚, at load eccentricity of 0B, 0.05B, 0.10B, and 0.15B, the US is 8.10, 8.08, 7.60, and 7.75 mm, respectively. Similarly, in the case of reinforced soil (u/B = 0.1), the US is 8.00, 7.81, 6.95, and 6.87 mm, respectively. A similar trend can be seen when u/B is 0.20, 0.30, 0.40, and 0.50. In Figure 7d, in the case of unreinforced soil, α = 30°, at load eccentricity of 0B, 0.05B, 0.10B, and 0.15B, the US is 5.10, 5.12, 5.10, and 5.30 mm, respectively. Similarly, in the case of reinforced soil (u/B = 0.1), the US is 5.52, 5.18, 5.05, and 5.05 mm, respectively. A similar trend can be seen when u/B is 0.20, 0.30, 0.40, and 0.50.

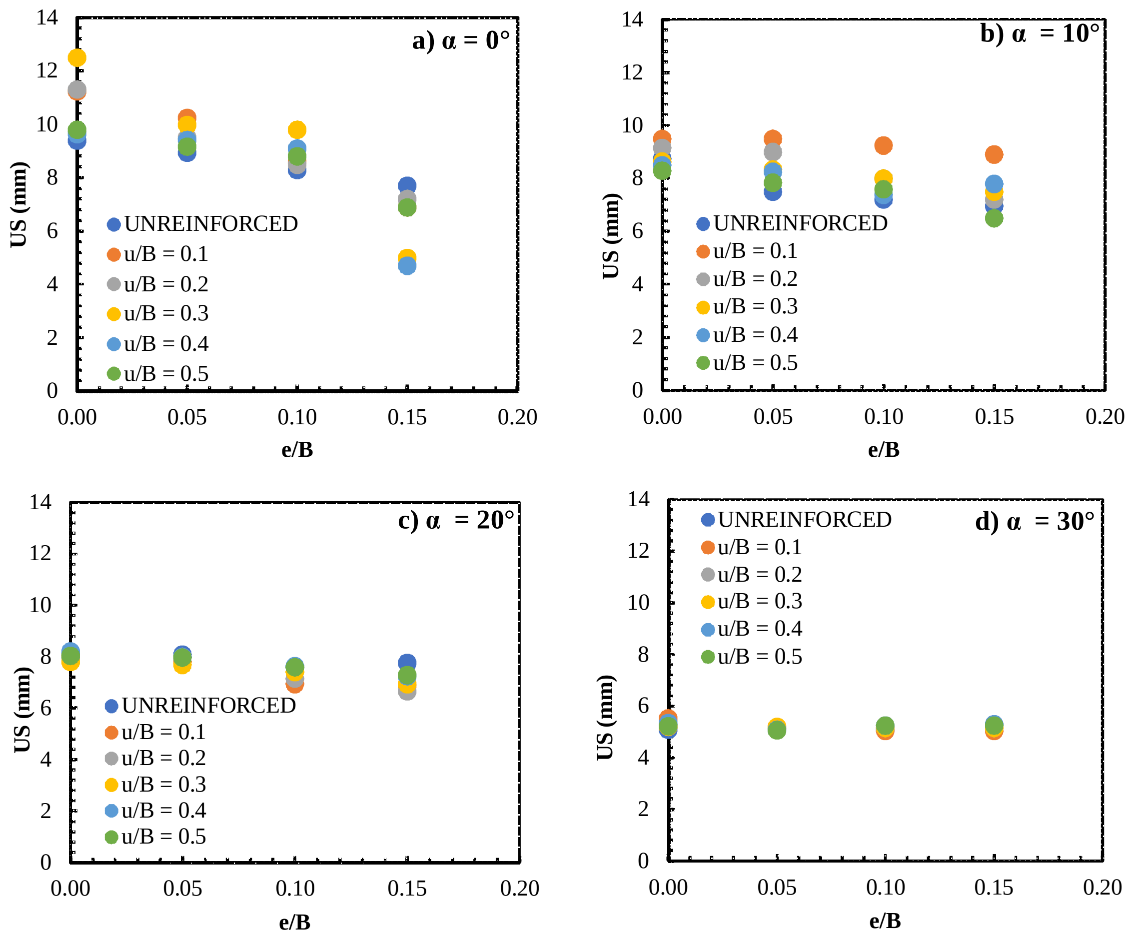

Figure 7. Effect of load eccentricity on the Ultimate settlement for different load inclinations; a) α = 0˚, b) α = 10˚, c) α = 20˚, and d) α = 30˚.

3.2.3. Effect of load eccentricity on footing tilt

Figure 8 a-d shows the effect of load eccentricity on the Footing tilt. It is obvious in Figure 8 that as the load eccentricity is increased the footing tilt keeps on increasing. For instance, Figure 8 a, in the case of unreinforced soil, α = 0°, at load eccentricity of 0B, 0.05B, 0.10B, and 0.15B, the footing tilt is 0, 0.12, 0.31, and 0.61 mm, respectively. Similarly, in the case of reinforced soil (u/B = 0.1), the footing tilt is 0, 0.09, 0.2, and 0.58 mm, respectively. A similar trend can be seen when u/B is 0.20, 0.30, 0.40, and 0.50. In Figure 8b, in the case of unreinforced soil, α = 10˚, at load eccentricity of 0B, 0.05B, 0.10B, and 0.15B, the footing tilt is 0.07, 0.09, 0.21, and 0.29 mm, respectively. Similarly, in the event of reinforced soil (u/B = 0.1), the footing tilt is 0.06, 0.18, 0.14, and 0.39 mm, respectively. A correspondence can be seen when u/B is 0.20, 0.30, 0.40, and 0.50. In Figure 8c, in the case of unreinforced soil, α = 20°, at load eccentricity of 0B, 0.05B, 0.10B, and 0.15B, the footing tilt is 0.10, 0.08, 0.23, and 0.32 mm, respectively. Similarly, in the occurrence of reinforced soil (u/B = 0.1), the footing tilt is 0.11, 0.06, 0.19, and 0.27 mm, respectively. A similar trend can be seen when u/B is 0.20, 0.30, 0.40, and 0.50. In Figure 8d, in the case of unreinforced soil, α = 30°, at load eccentricity of 0B, 0.05B, 0.10B, and 0.15B, the footing tilt is 0.03, 0.03, 0.09, and 0.16 mm, respectively. Surprisingly, in the case of reinforced soil (u/B = 0.1), the footing tilt at 0B is -0.00114, which indicates that the tilt occurs in the opposite direction. A corresponding trend can be seen when u/B is 0.20, 0.30, 0.40, and 0.50 for 0.04, 0.09, and 0.16 mm, respectively. A related pattern can be seen when u/B is 0.20, 0.30, 0.40, and 0.50.

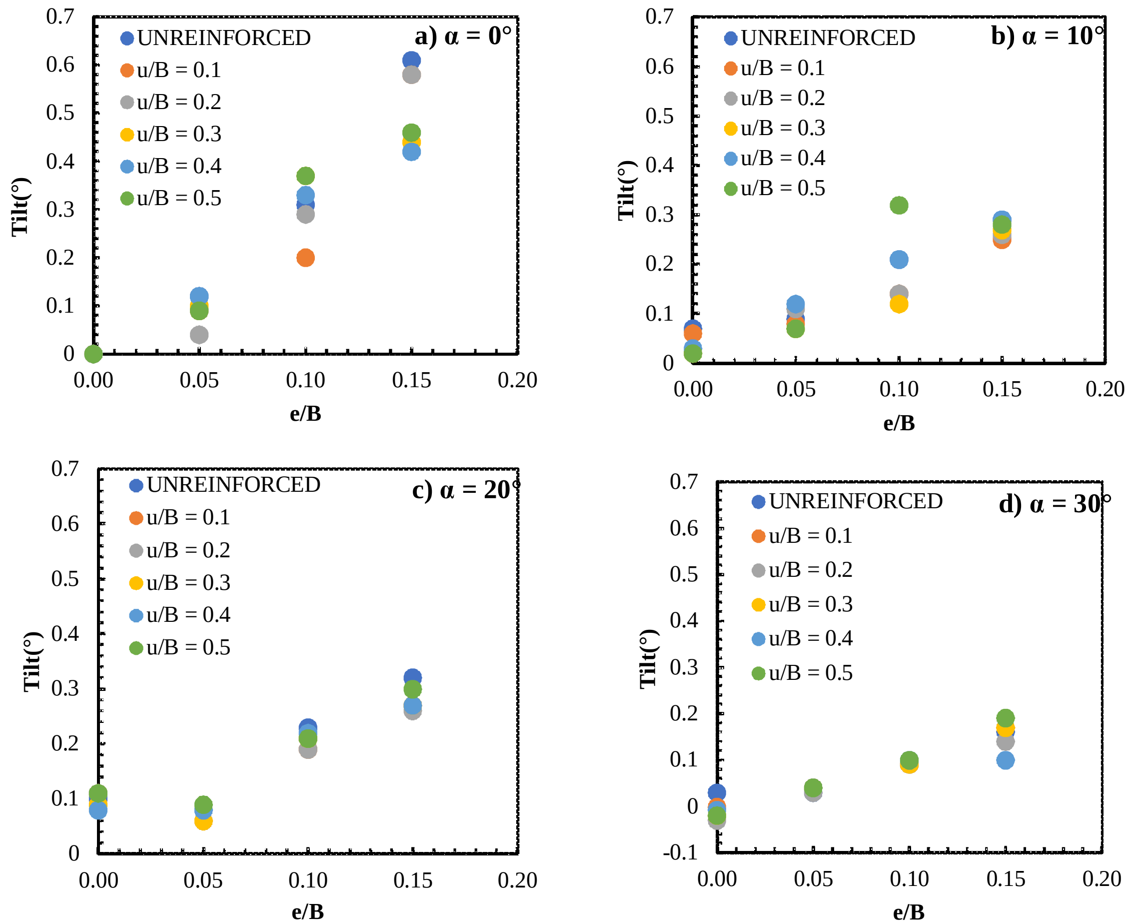

Figure 8. Influence of load eccentricity on the footing tilting for different load inclinations; a) α = 0˚, b) α = 10˚, c) α = 20˚, and d) α = 30˚.

3.2.4. Effect of load eccentricity on HD

Figure 9 a-c shows the influence of load eccentricity on the HD. It is apparent in Figure 9 that as the load eccentricity is increased the HD keeps on decreasing. For instance, Figure 9a, in the case of unreinforced soil, α = 10˚, at load eccentricity of 0B, 0.05B, 0.10B, and 0.15B, the HD is 3.10, 3.00, 2.80, and 2.40 mm, respectively. Similarly, in the case of reinforced soil (u/B = 0.1), the HD is 4.20, 3.50, 3.00, and 2.60 mm, respectively. A corresponding pattern can be seen when u/B is 0.20, 0.30, 0.40, and 0.50. In Figure 9b, in the case of unreinforced soil, α = 20˚, at load eccentricity of 0B, 0.05B, 0.10B, and 0.15B, the HD is 6.13, 4.73, 5.62, and 5.49 mm, respectively. Similarly, in the case of reinforced soil (u/B = 0.1), the HD is 5.79, 5.99, 5.18, and 4.76 mm, respectively. A related pattern can be seen when u/B is 0.20, 0.30, 0.40, and 0.50. In Figure 9c, in the case of unreinforced soil, α = 30˚, at load eccentricity of 0B, 0.05B, 0.10B, and 0.15B, the HD is 4.79, 4.95, 5.05, and 4.97 mm, respectively. There is a slight increase in the HD as the eccentricity increases from 0B to 0.05B. The increase in the values is very negligible. The HD is constant throughout 0.05 B, 0.10B, and 0.15 B. Similarly, in the case of reinforced soil (u/B = 0.1), the HD is 4.77, 5.01, 4.85, and 5.05 mm, respectively. A parallel pattern can be seen when u/B is 0.20, 0.30, 0.40, and 0.50.

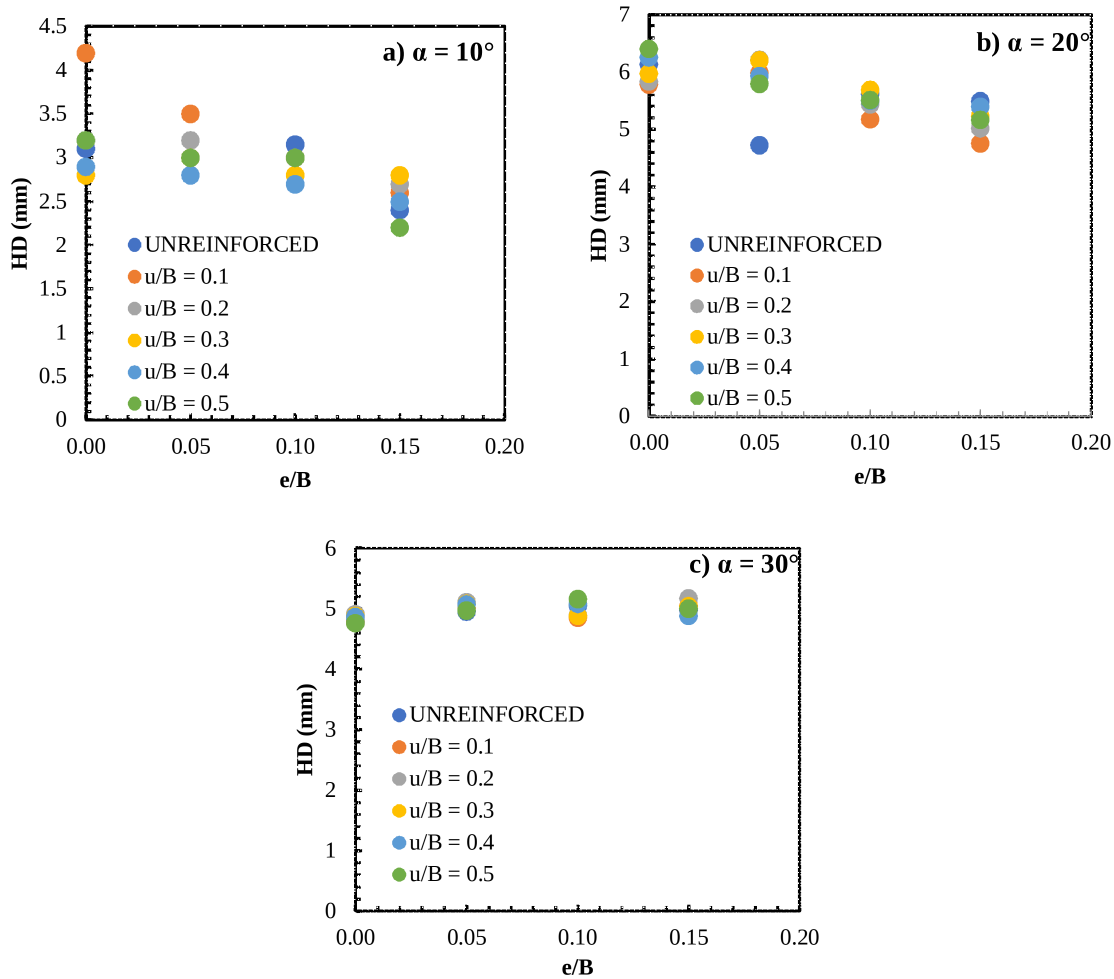

Figure 9. Influence of load eccentricity on the footing horizontal displacement for different load inclinations; a) α = 10˚, b) α = 20˚, and c) α = 30˚.

3.3. Effect of geo-grid location

3.3.1. Effect of geo-grid location on UL

Figure 10 a-d shows the influence of geo-grid location on the UL. Observations from Figure 10 a-b, which represents α = 0˚ and 10˚ that the UL for reinforced soil (u/B = 0.1) is 278 and 235 kN/m, respectively, and for unreinforced soil, the UL is 249 and 200 kN/m, respectively. On further increasing the depth of geogrid, the UL decreases. Similarly, in Figure 10 c-d (α = 20˚ and 30˚) the geo-grid reinforcement is futile as no change in UL can be observed for the varying locations. This means that when the load inclination is over and above 20˚, there is hardly any effect of geogrid. This may be because of the fact that the shear pattern below the footing gets distorted when load is not vertical concentric. As for the increase in eccentricity, the UL decreases in all Figure 10 a-d. The optimum location for the ultimate load is at 0.1B.

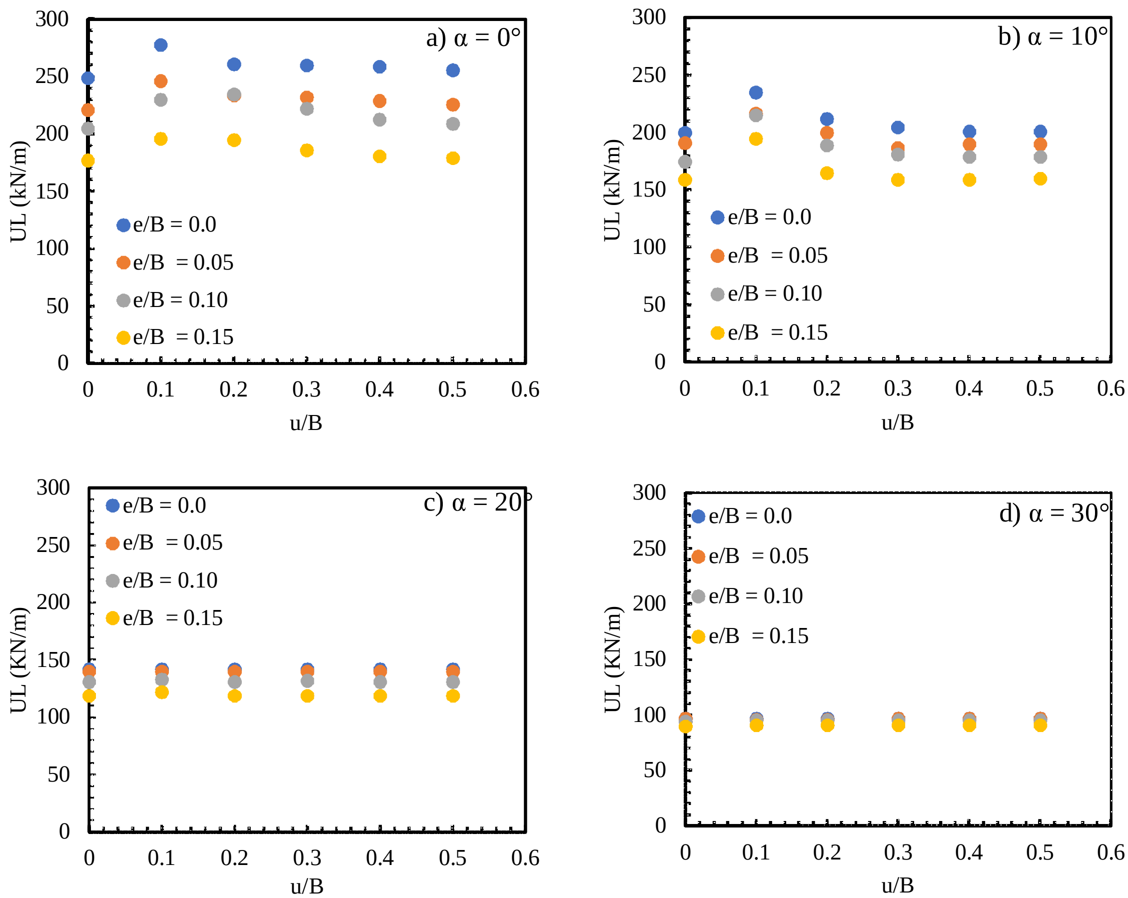

Figure 10. Impact of geo-grid location on ultimate load for the various load inclinations; a) α = 0˚, b) α = 10˚, c) α = 20˚, and d) α = 30˚.

3.3.2. Effect of geo-grid location on US

Figure 11a-d shows the impact of geogrid location on the US. It can be seen from the Figure 11a, α = 0˚, e/B = 0.0 and 0.05, the US first increases up to u/B = 0.10, and thereafter, it starts dipping. In Figure 11b, a similar trend can be seen, however; the settlement values for different eccentricities are very close to each other. In contrast, when load inclination is over and above 20˚, the US values kept on decreasing as the geo-grid depth is increased. This phenomenon can be observed in Figure 11c and d.

3.3.3. Effect of geo-grid location on footing tilt

Figure 12a-d shows the influence of geogrid location on the Footing tilt. In Figure 12a, α = 0˚, the footing tilt for e/B = 0.0 and e/B = 0.05 increase from unreinforced to 0.2B, and subsequently, decrease all the way to 0.5B. From Figure 12b, α = 10˚ for all eccentricity, the footing tilt increases with a large margin from unreinforced to 0.1B then decreases at 0.2B and remains at a constant value. In Figure 12c, α = 20˚, the geogrid locations only have a minute difference in footing tilt values which result in a constant. Figure 12d, α = 30˚, represents the footing tilt – geo-grid location with no change therefore making it a negligible progression.

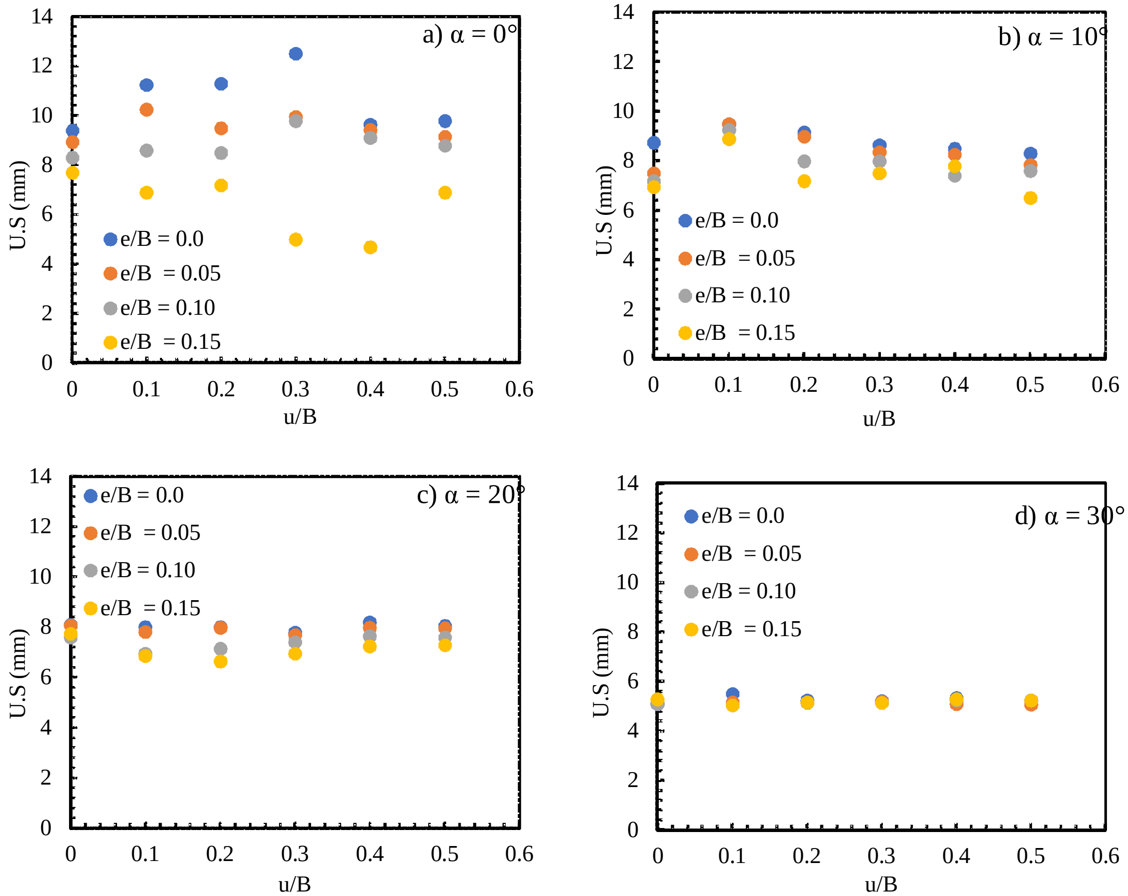

Figure 11. Impact of geo-grid location on the ultimate settlement for different load inclinations; a) α = 0˚, b) α = 10˚, c) α = 20˚, and d) α = 30˚.

3.3.4. Effect of geo-grid location on HD

Figure 13a-d shows the influence of geogrid location on the HD, Figure 13a, α = 0˚, the e/B = 0.15, HD is constant for 0.0B to 0.02B and sharp decreases to 0.3B and remains constant up to 0.5B. e/B = 0.10 decreases for 0.1B then increases largely for 0.2B, and remains constant up to 0.5B. For e/B = 0.05, the pattern is constant. For α = 10˚, 20˚, and 30˚, the pattern remains constant with a nuance in change. However, it was observed that for e/B = 0.15, the tilt had maximum values in comparison to other eccentricities.

4. Validation of Numerical Modelling

As the present study is purely numerical in nature and to make it applicable for field application, field experimental study is important. However, due to numerous constraints, be it the funding or availability of proper testing facility it was not feasible to conduct field investigations for the present study. However, on the bright side, for the validation, the numerical model results can be compared with the existing literature. Therefore, the results of a published work in the past is selected [22] and compared with the present study (Figure 14). It can be seen in Figure 14 that the results obtained from the present study and the literature are showing the same pattern. Owing to the material properties, size of the footing and the geometry of the soil extent, the actual result values obtained in the present study and the literature will, in-fact, differ.

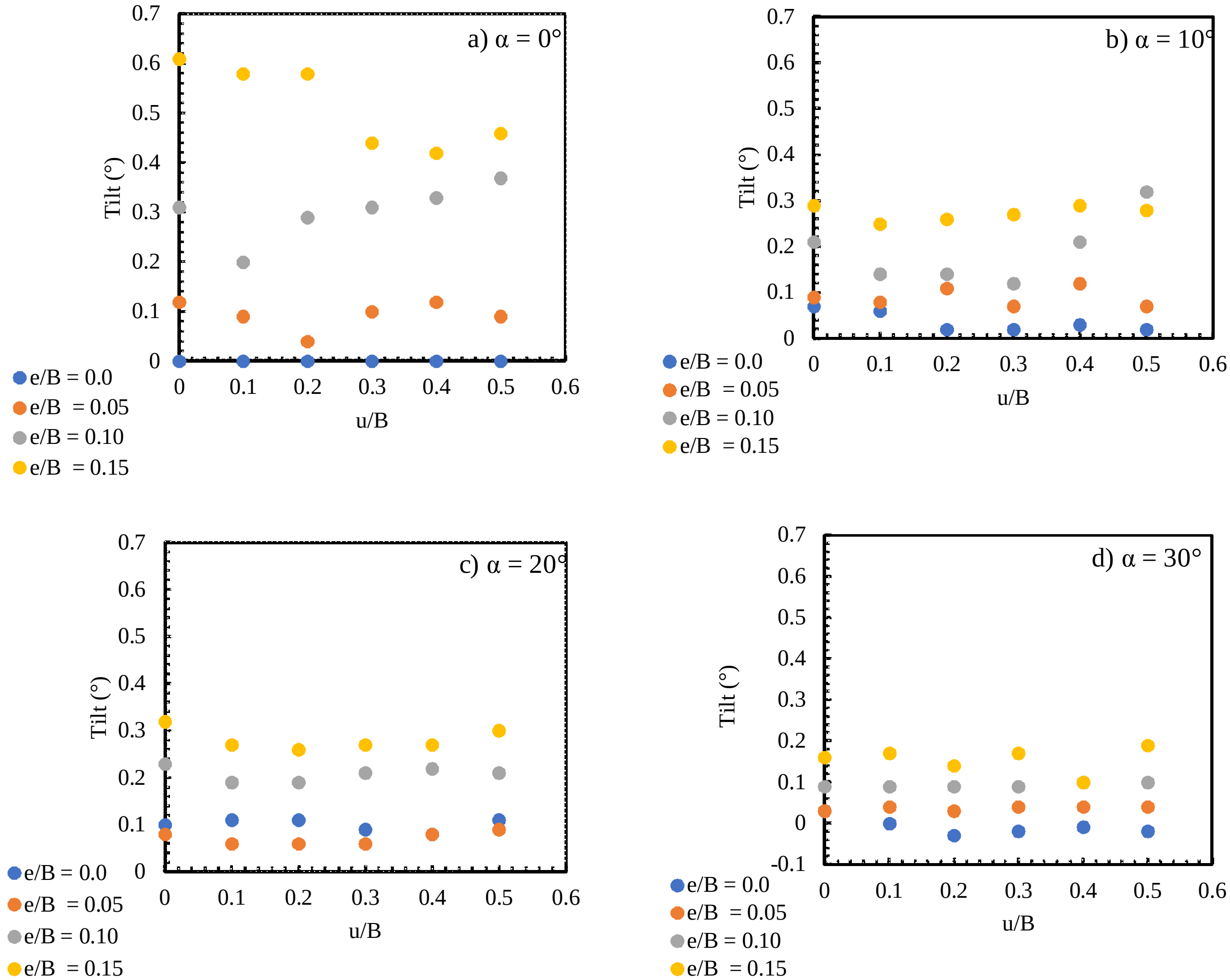

Figure 12. Effect of geo-grid location on the footing tilting for different load inclinations; a) α = 0˚, b) α = 10˚, c) α = 20˚, and d) α = 30˚.

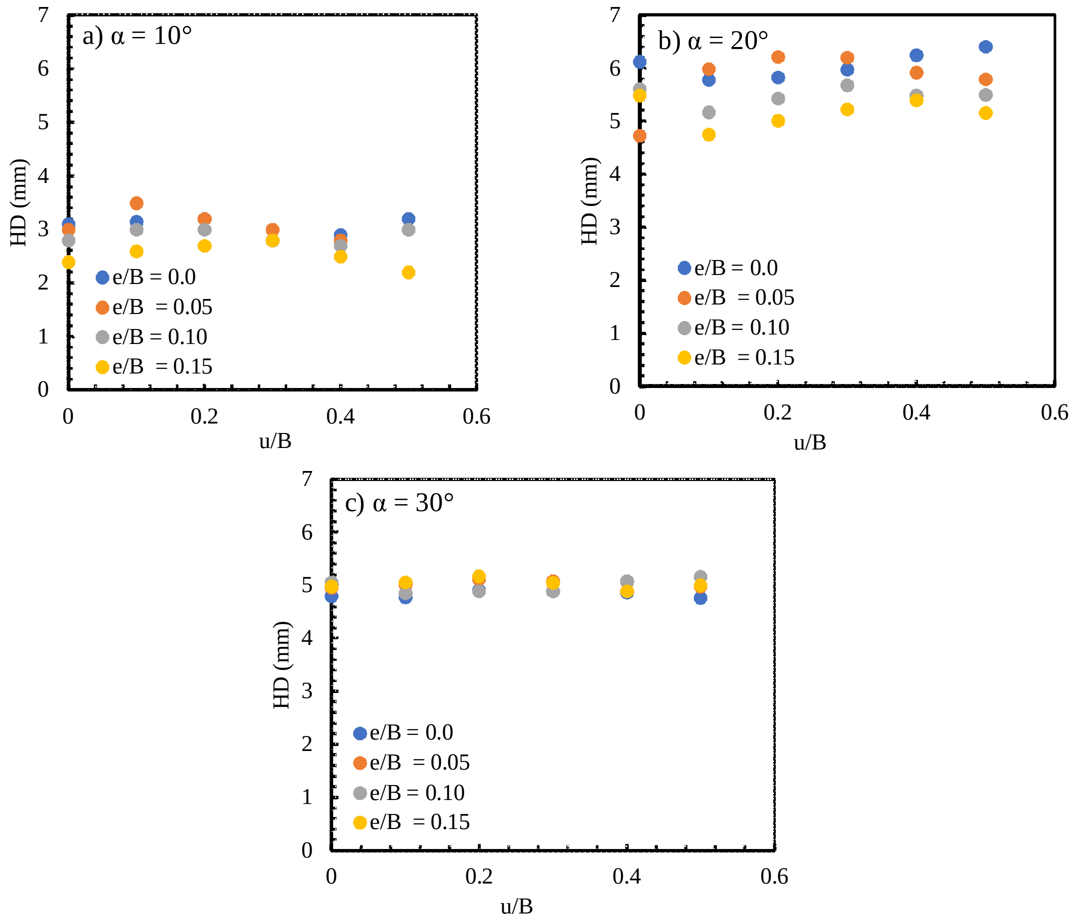

Figure 13. Influence of geo-grid location on the footing horizontal displacement for different load inclinations; a) α = 10˚, b) α = 20˚, and c) α = 30˚.

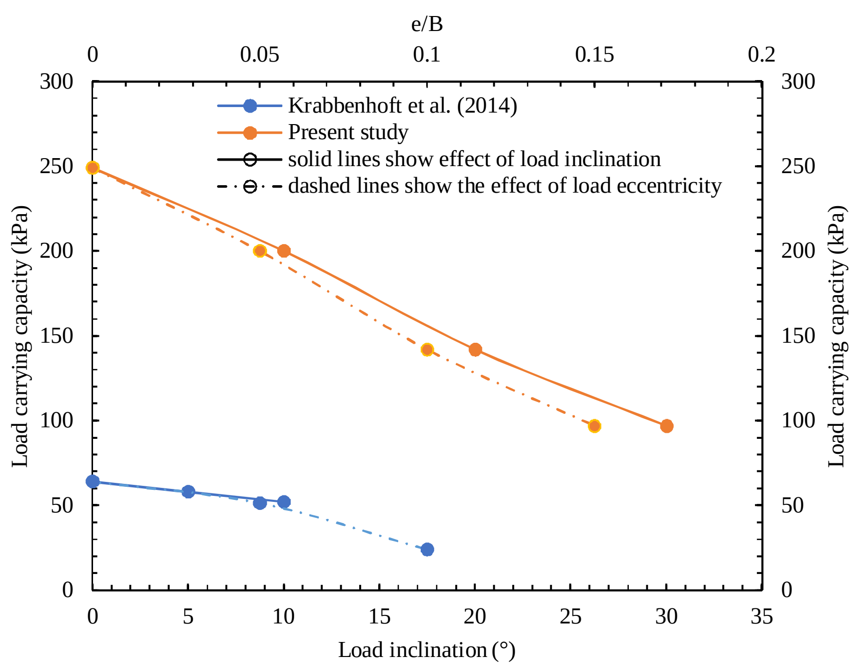

Figure 14. Comparison of the present study with the literature.

5. Conclusions

- Load eccentricity has significantly affected the footing's UL, which explains, when the load eccentricity increases the footing UL decreases. For instance, in the case of unreinforced soil, $\alpha = 0^\circ$, at load eccentricity of 0B, 0.05B, 0.10B, and 0.15B, the UL is 249, 221, 205, and 177 kN/m, respectively. Similarly, in the case of reinforced soil (u/B = 0.1), the UL is 278, 246.5, 230, and 196 kN/m, respectively.
- With the load eccentricity is increased the US keeps on decreasing. For instance, in the case of unreinforced soil, $\alpha = 0^\circ$, at load eccentricity of 0B, 0.05B, 0.10B, and 0.15B, the US is 9.40, 8.95, 8.30, and 7.70 mm, respectively.
- As load eccentricity is increased the tilt keeps on increasing. For instance, in the case of unreinforced soil, $\alpha = 0^\circ$, at load eccentricity of 0B, 0.05B, 0.10B, and 0.15B, the footing tilt is 0, 0.12, 0.31, and 0.61 mm, respectively.
- When load eccentricity is increased the HD keeps on decreasing. For instance, in the case of unreinforced soil, $\alpha = 10^\circ$, at load eccentricity of 0B, 0.05B, 0.10B, and 0.15B, the HD is 3.10, 3.00, 2.80, and 2.40 mm, respectively.
- When load inclination increases the UL keeps on decreasing. For instance, in the case of unreinforced soil, u/B= 0, at load inclination of $\alpha = 0^\circ$, $\alpha = 10^\circ$, $\alpha = 20^\circ$, $\alpha = 30^\circ$, the UL is 249, 200, 142, and 97 kN/m, respectively.
- If the load inclination is increased the US keeps on decreasing. For instance, in the case of unreinforced soil, e/B= 0.0, at an inclination of $\alpha = 0^\circ$, $\alpha = 10^\circ$, $\alpha = 20^\circ$, $\alpha = 30^\circ$, the US is 9.4, 8.75, 8.1, and 5.1 mm, separately.
- As the load inclination increases, the footing tilting keeps on increasing from $\alpha = 0^\circ$ to $\alpha = 20^\circ$, and it sharply decreases at $\alpha = 30^\circ$. For instance, in the case of unreinforced soil, u/B = 0, at load inclination of $\alpha = 0^\circ$, $\alpha = 10^\circ$, $\alpha = 20^\circ$, $\alpha = 30^\circ$, the footing tilt is 0°, 0.07°, 0.1°, and 0.03°, respectively.
- As the load inclination increases the HD keeps on increasing to $\alpha = 0^\circ$ and then decreases at $\alpha = 30^\circ$. For instance, in the case of unreinforced soil, u/B= 0, at load inclination of $\alpha = 0^\circ$, $\alpha = 10^\circ$, $\alpha = 20^\circ$, $\alpha = 30^\circ$, the HD is 0, 3.1, 6.13, and 4.79 mm, respectively.
- As the UL reaches 0.1B, which is 278 and 235 kN/m, respectively, and the unreinforced is 249 and 200 kN/m. After 0.1B the UL decreases and the optimum location for the ultimate load is at 0.1B.
- For all eccentricity the US increases with a large margin from unreinforced to 0.1B then decreases at 0.2B, and remains at a constant and geo-grid locations only have a minute difference in US values, which result in a constant.
- The u/B only have a minute difference in US values, which results in a constant. The US – u/B shows no change, therefore, making it a negligible progression. As the u/B increases, the HD remains constant and sharply decreases and remains constant up to 0.5B. The distance between the eccentricities becomes negligible as the u/B increases.
- As the geo-grid is introduced in the unreinforced soil, the footing tilting decreases significantly. Moreover, independent of geogrid location, the footing tilt keeps on decreasing as the load inclination is increased. For unreinforced case, e/B = 0.05 the footing tilting for different load inclinations, i.e. $\alpha = 0^\circ$, 10°, 20°, and 30° was 0.12, 0.09, .08, and 0.03, respectively. For the same load eccentricity, but with geo-grid reinforcement (u/B = 0.1), the footing tilting values were 0.09, 0.08, 0.06 and 0.04.

Acknowledgements

The authors would like to thank the Laboratory staff of the Lovely Professional University for providing the required support to conduct this study.

References

[1]. Tahmasebipoor, A. Noorzad, R. Shooshpasha, E. and Barari, A. (2010). A parametric study of stability of geotextile-reinforced soil above an underground cavity. Arabian Journal of Geosciences 5, 449–456.

[2]. Cooper, A. H. and Saunders, J. M. (2002). Road and bridge construction across gypsum karst in England. Engineering Geology 65, 217–223.

[3]. Fiore, A. Fazio, N. L. Lollino, P. Luisi, M. Miccoli, M. N. Pagliarulo, R. Perrotti, M. Pisano, L. Spalluto, L. Vennari, C. and Vessia, G. (2018). Evaluating the susceptibility to anthropogenic sinkholes in Apulian calcarenites, southern Italy. Geological Society Special Publication, 466, 381–396.

[4]. Yang, Z. Yue, Z. and Li, L. (2011). Design, construction, and mechanical behavior of relics of complete large Longyou rock caverns carved in argillaceous siltstone ground. Journal of Rock Mechanics and Geotechnical Engineering, 3, 131–152.

[5]. Vattano, M. Parise, M. Lollino, P, Bonamini, M, Maggio, D. and Madonia, G. (2013). Examples of Anthropogenic Sinkholes in Sicily and Comparison with Similar Phenomena in Southern Italy. In: 13th sinkhole conference. 263–271.

[6]. Van Den Eeckhaut, M. Poesen, J. Dusar, M. Martens, V. and Duchateau, P. (2007). Sinkhole formation above underground limestone quarries: A case study in South Limburg (Belgium). Geomorphology 91, 19–37.

[7]. Parise, M. and Lollino, P. (2011). A preliminary analysis of failure mechanisms in karst and man-made underground caves in Southern Italy. Geomorphology 134, 132–143.

[8]. Li, L.H. Yang, Z. F. Yue, Z. Q. and Zhang, L. Q. (2009). Engineering geological characteristics, failure modes and protective measures of Longyou rock caverns of 2000 years old. Tunneling and Underground Space Technology 24, 190–207.

[9]. Bétournay, M. C. (2009). Abandoned metal mine stability risk evaluation. Risk Analysis 29, 1355–1370.

[10]. Castellanza, R. Lollino, P. and Ciantia, M. (2018). A methodological approach to assess the hazard of underground cavities subjected to environmental weathering. Tunneling and Underground Space Technology 82, 278–292.

[11]. Song, K. I. Cho, G. C. and Chang, S. B. (2012) Identification, remediation, and analysis of karst sinkholes in the longest railroad tunnel in South Korea. Engineering Geology 135–136, 92–105.

[12]. Kim, S. Kim, T. Shin, D. and Kwon, H. (2009). A Study on the Development of Rapidly Hardening Grouting Method for the Effective Filling in the Underground Cavity. Tunnel & Underground Space

[13]. Zhao, Y. Li, P. and Tian, S. (2013) Prevention and treatment technologies of railway tunnel water inrush and mud gushing in China. Journal of Rock Mechanics and Geotechnical Engineering 5, 468–477.

[14]. Liu, L. Shi, Z. Tsoflias, G. P. Peng, M. Liu, C. Tao, F. and Liu, C. (2021). Detection of karst cavity beneath cast-in-place pile using the instantaneous phase difference of two receiver recordings. Geophysics 86, 27–38.

[15]. Del Prete, S. and Parise, M. (2013). In: P16th International Congress of Speleology, Czech Republic, Brno. 236–241.

[16]. Mazouz, B. Mansouri, T. Baazouzi, M. and Abbeche, K. (2022). Assessing the Effect of Underground Void on Strip Footing Sitting on a Reinforced Sand Slope with Numerical Modeling. Engineering, Technology & Applied Science Research 12, 9005–9011.

[17]. Jao, M. and Wang, M. C. (1998). Stability of strip footings above concrete-lined soft ground tunnels. Tunnelling and Underground Space Technology, 13, 427–434.

[18]. Shrestha, S. Baral, P. Bergado, D. T. Chai, J. C. and Hino, T. (2014) Numerical simulations using FEM 2D compared to FEM 3D and observed behavior of reinforced full-scale embankment. In: 9th International Symposium on Lowland Technology, 85-92.

[19]. Sharma, V. Kumar, A. and Kapoor, K. (2019). Sustainable deployment of crushed concrete debris and geotextile to improve the load carrying capacity of granular soil. Journal of Cleaner Production, 228, 124–

[20]. Sharma, V. and Kumar, A. (2023). Plate Load Tests on the Ring and Circular Footings. Lecture Notes in Civil Engineering, 280, 209–217.

[21]. Sharma, V. and Kumar, A. (2022) Behavior of eccentrically and obliquely loaded ring footing resting on geocell-reinforced sand. Innovative Infrastructure Solutions, 7, 1–18.

[22]. Krabbenhoft, S. Damkilde, L. and Krabbenhoft, K. (2014). Bearing Capacity of Strip Footings in Cohesionless Soil Subject to Eccentric and Inclined Loads. International Journal of Geomechanics,

مطالعه عددی رفتار پایه نواری با شیب غیرعادی که در بالای توده خاکی حاوی فضای خالی قرار دارد

وایبهاو شارما*، اندی کوامه یبوآ، جاشوا آساره، ناتیلیو پیلای و جاسپریت سینگ

دانشگاه حرفه‌ای لاولی، فاگورا، پنجاب، هند

ارسال 2023/05/16، پذیرش 2023/06/06

* نویسنده مسئول مکاتبات: civil.vaibhav.sharma@gmail.com

چکیده:

وجود هر گونه حفره زیرزمینی در لایه خاک می تواند به طور جدی به عملکرد ساختاری تأسیسات پوشاننده آسیب برساند. اینها ممکن است به دلیل شبکه‌های معدن، تونل، آب و گاز یا کانال‌های قدیمی ایجاد شوند. در تحقیق حاضر، یک فضای خالی مدور در نظر گرفته شده و اثر آن بر روی پایه نوار سطحی (به شکل بار نهایی (UL)، نشست نهایی (US)، کج شدن پایه و جابجایی افقی پایه (HD)) با استفاده از آن مورد بررسی قرار گرفته است. شبیه سازی عددی پارامترهای متغیر عبارتند از خروج از مرکز بار (e)، شیب بار (α) و محل تقویت ژئوگرید (u). مشاهده می‌شود که با افزایش تمایل بار و خروج از مرکز، UL کاهش می یابد. به عنوان مثال، در خاک تقویت نشده، u/B = 0، در شیب بار = 0 درجه، 10 درجه، 20 درجه و 30 درجه، UL به ترتیب 249، 200، 142 و 97 کیلو نیوتن بر متر است. علاوه بر این، با تغییر مکان ژئوشبکه، ابتدا UL هنگامی که در نزدیکی پایه قرار می‌گیرد افزایش می‌یابد (u/B = 0.10)، و پس از آن، با افزایش فاصله بین پایه و ژئوشبکه شروع به کاهش می‌کند. به عنوان مثال، UL 249، 278، 267، 260، 259، و kN/m 256 است که e/B = 0.0، α = 0 درجه، و u/B از 0 تا 0.5 با افزایش 0.1 تغییر می‌کند. با افزایش خروج از مرکز، کج شدن افزایش می‌یابد. به عنوان مثال، u/B = 0.0 برای α = 0 درجه؛ مقادیر کج شدن 0 درجه، 0.12 درجه، 0.31 درجه و 0.61 درجه است. علاوه بر این، با افزایش خروج از مرکز بار، HD کاهش می‌یابد (برای u/B = 0.1 و α = 10 درجه، HD به ترتیب 4.20، 3.5، 3.00 و 2.60 میلی متر است).

کلمات کلیدی: خاک پنبه سیاه، مواد زائد، درجه فرعی، CBR، IIT PAVE.